# A boundary error sensing arrangement for virtual sound barriers to reduce noise radiation through openings

Shuping Wang,[1a)] Jiancheng Tao,[2] Xiaojun Qiu,[1] Jie Pan[3]

[1] Centre for Audio, Acoustics and Vibration, Faculty of Engineering and IT, University of Technology Sydney, NSW 2007, Australia

[2] Key Laboratory of Modern Acoustics and Institute of Acoustics, Nanjing University, Nanjing 210093, China

[3] Department of Mechanical Engineering, The University of Western Australia, WA 6009, Australia

Suggested running title: Boundary error sensing strategy

a) Author to whom correspondence should be addressed. Electronic mail: shuping.wang@uts.edu.au.

# ABSTRACT

Previous work has demonstrated that sound radiation through a cavity opening can be reduced with secondary sources at the edge of the opening, but the error microphones are implemented over the entire opening, which might affect the natural ventilation, lighting, and especially the access through the opening in some applications. A boundary error sensing arrangement is proposed and investigated in this paper. It is found that a double-layer error microphone arrangement achieves better performance than a single-layer one. Although its performance is not as good as the arrangement with error microphones distributed over the entire opening, it is preferable in some applications because it does not block the opening. It is also found that there exists an upper-limit frequency for the systems with error microphones installed at the edge, which is related to the size of the opening and can be increased by adding more layers of error microphones at the edge. This work demonstrates the possibility of developing an almost invisible virtual sound barrier system that can block sound transmission through an opening without affecting its functionalities.

PACS numbers: 43.50.Ki

## I. INTRODUCTION

Openings are important for lighting, natural ventilation, and access through buildings and enclosures; however, they introduce sound transmission paths that reduce the transmission loss of the whole structures. Traditional passive noise control methods, such as applying porous materials, micro-perforated absorbers, and quarter-wave resonators, require that the opening be sealed and/or filled with these materials or structures, so they are inappropriate for some applications.[1–3] Compared with passive noise control, active noise control (ANC) can maintain the functionalities of the openings and works effectively, especially for low-frequency noise.

Using Huygens' principle as the theoretical basis, it has been demonstrated in previous work that sound power radiation through openings to the outside can be effectively reduced by placing a sufficient number of secondary sources over the entire opening.[4–8] To avoid putting secondary sources in the middle of the opening, a double-layer secondary source system at the edge of the opening has been proposed and both the numerical simulation and experiment results demonstrate the feasibility of this configuration.[9] Due to reciprocity, applying secondary sources only on the frame of the opening can also reduce sound radiation through the opening to inside the cavity.[10] However, in these systems, error microphones are located over the entire opening, which might affect access through the opening.

To achieve global sound power reduction, error microphones should provide information that is proportional to the sound power of the system. The sound power can be measured according to ISO 3744 with ten or twenty microphones on a hemisphere.[11-12] The hemisphere's radius should be larger than each of the three values: twice the largest source dimension, a quarter of the wavelength of interest, and 1 m.[11] Therefore, it is not practical to apply error microphones at these locations in some applications, especially for a large noise source in some applications where a compact system is desired. Since sound power is the integral of sound intensity over a surface around the noise source, Berry *et al.* used the near-field sound intensity as the cost function, but finds that due to its signed quantity, there are difficulties associated with sound intensity minimization.[13]

In order to achieve effective global control with error microphones in the near field, their positions need to be optimized. The optimal positions for error microphones are the locations where noise reduction is the greatest when minimizing the total radiated sound power.[14] Shafer *et al.* demonstrated experimentally that the measured near-field sound pressure map approximates the one when minimizing the sound power if the error microphones are at these ideal positions and that moving them to other locations will greatly deteriorate the sound power reduction performance.[15]

There has been much work reported on optimizing the positions of error microphones. For simple cases like using a single-channel ANC system to reduce the primary noise generated by a monopole or dipole, the optimal positions can be investigated theoretically.[16] If the primary sound field is complicated, genetic algorithms and simulated annealing algorithms can be used to search for the optimal positions of error microphones, but it is usually difficult to obtain the global optimal solution and the optimal solutions might be different for noise at different frequencies.[17–19]

Virtual sensing is another way to achieve effective noise control with error microphones in the near field. In this strategy, physical error microphones near the primary source are used to estimate the sound pressures at virtual error sensor locations in the far field for minimization.[20] If the virtual error sensors are at the locations defined in ISO 3744, the sound power of the system can be minimized. However, most previous work on virtual sensing focuses on local control, and its feasibility to achieve global sound power reduction remains to be investigated.[21–23] Another problem with the virtual sensing approach is that it requires preliminary identification of the system.

In this paper, a simple configuration of error microphones is proposed that installs error microphones at the edge of the cavity opening. The performances of single-layer and double-layer error microphones at the edge are compared. The upper-limit frequency of effective noise control for such a boundary error microphone arrangement and its relationship with the opening size are explored.

## II. THEORY

Schematic diagrams of the single-layer and double-layer error microphone arrangements are shown in Fig. 1. In the single-layer system, the error microphones are distributed along the edge of the opening. In the double-layer system, two layers of error microphones are installed at two different heights along the edge, and they have the same $x$–$y$ coordinates. All the five walls of the cavity are rigid, so sound outside the cavity is solely that transmitted through the opening. The primary noise source is assumed to be a monopole point source inside the cavity.

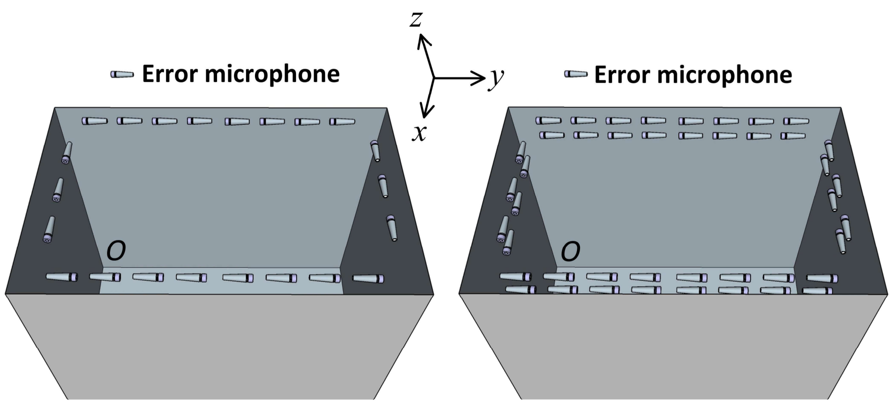


(a) (b)

FIG. 1. (Color online) Schematic diagrams of (a) single-layer error microphones at the edge and (b) double-layer error microphones at the edge.

The sum of the squared sound pressures at all the error microphones with a control effort constraint is defined as the cost function[4]

$$J = \mathbf{p}^{\mathrm{H}}\mathbf{p} + \beta \mathbf{q}_{\mathrm{s}}^{\mathrm{H}}\mathbf{q}_{\mathrm{s}}, \quad (1)$$

where $\mathbf{p}$ is the vector of sound pressures at the error points, $\mathbf{q}_{\mathrm{s}}$ is the vector of the strengths of secondary sources, and $\beta$ is a real number to constrain the outputs of secondary sources.[24] After minimizing Eq. (1), the optimized strengths of the secondary sources can be obtained with

$$\mathbf{q}_{\mathrm{s}} = -(\mathbf{Z}_{\mathrm{se}}^{\mathrm{H}}\mathbf{Z}_{\mathrm{se}} + \beta\mathbf{I})^{-1}\mathbf{Z}_{\mathrm{se}}^{\mathrm{H}}\mathbf{Z}_{\mathrm{pe}}q_{\mathrm{p}}\,, \qquad (2)$$

where $\mathbf{Z}_{\mathrm{se}}$ is the acoustic transfer function matrix between the secondary sources and the error microphones, $\mathbf{Z}_{\mathrm{pe}}$ is the acoustic transfer function vector from the primary source to the error microphones, and $q_{\mathrm{p}}$ is the strength of the primary source.

The noise reduction of the system is defined as the difference between the sound power levels of the system with and without control

$$\mathrm{NR} = 10\log_{10}\frac{W_{\mathrm{off}}}{W_{\mathrm{on}}}\,, \qquad (3)$$

where $W_{\mathrm{off}}$ and $W_{\mathrm{on}}$ are the sound powers of the system without and with control, respectively. The sound power $W_{\mathrm{off}}$ can be calculated as the integral of sound intensity over the opening area $S$

$$W_{\mathrm{off}} = \frac{1}{2}\iint_S \mathrm{Re}\left\{p_{\mathrm{po}}{}^{*}v_{\mathrm{po}}\right\}\mathrm{d}S\,, \qquad (4)$$

where $p_{\mathrm{po}}$ and $v_{\mathrm{po}}$ are the sound pressure and normal particle velocity generated by the primary source at the opening. The sound power $W_{\mathrm{on}}$ is the sum of the contributions of the primary source and all the secondary sources

$$W_{\mathrm{on}} = \frac{1}{2}\iint_S \mathrm{Re}\left\{[p_{\mathrm{po}} + p_{\mathrm{so}}]^{*}[v_{\mathrm{po}} + v_{\mathrm{so}}]\right\}\mathrm{d}S\,. \qquad (5)$$

In Eq. (5), $p_{\mathrm{so}}$ and $v_{\mathrm{so}}$ are the sound pressure and normal particle velocity generated by the secondary sources with the optimized strengths $\mathbf{q}_{\mathrm{s}}$, which are calculated with Eq. (2).

## III. SIMULATIONS AND DISCUSSIONS

**A. Comparison between single-layer and double-layer error microphones at the edge**

In the simulations, the dimensions of the open cavity are 0.3 m × 1.0 m × 0.598 m ($l_x \times l_y \times l_z$), and the size of the opening is 0.3 m × 1.0 m. The modal superposition method in Ref. [8] is applied to obtain the theoretical acoustic transfer functions and the sound pressure and particle velocity at the opening to calculate the sound power of the system. The primary source is a monopole point source at (0.01, 0.01, 0.01) m with a strength of $q_{\mathrm{p}} = 2\times10^{-4}$ m$^3$/s. The secondary sources are also monopole point sources, and forty-four of them are evenly distributed at the height of $z$ = 0.448 m.

Numerical simulations show that the number of error microphones in single-layer and double-layer systems does not significantly affect the noise reduction performance if the number of error microphones is larger than that of secondary sources to prevent the system from being underdetermined, so more error microphones than secondary sources are used in the simulations. A total of 56 error microphones in the single-layer and double-layer systems are applied at the opening, and their positions are shown in Figs. 2(a) and (b). The results for the traditional arrangement of evenly distributed error microphones, shown in Fig. 2(c), are also given for comparison. The error microphones in the single-layer and evenly distributed systems are at the height of $z$ = 0.588 m, and those in the double-layer system are at $z$ = 0.568 m and $z$ = 0.588 m planes.

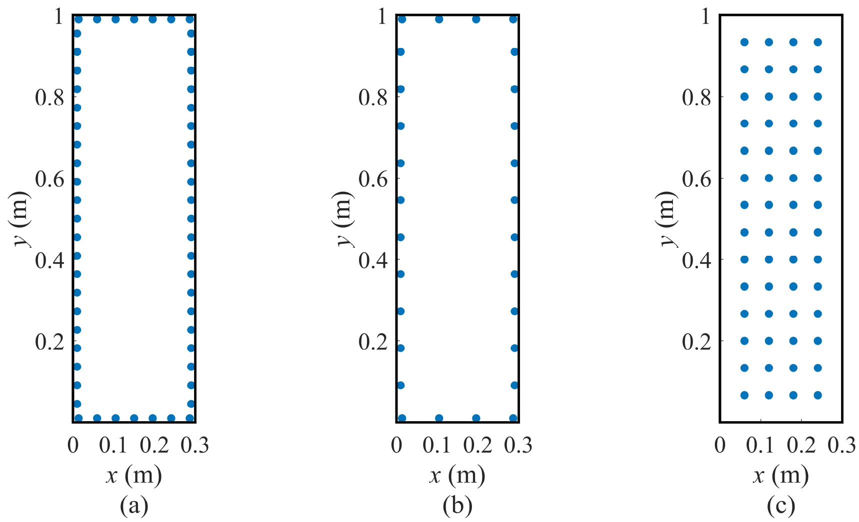


FIG. 2. (Color online) The positions of error microphones in the *x*-*y* plane: (a) single-layer error microphones at the edge, (b) one of the layers of the double-layer error microphones at the edge, and (c) evenly distributed error microphones.

The sound power levels of the system with and without ANC are shown in Fig. 3. The theoretically best noise reduction performance obtained by minimizing the sound power is also included for comparison.[24] It can be seen that the evenly distributed error microphones achieve the highest noise reduction, and that the double-layer error microphones perform better than the single-layer ones. Taking 1000 Hz as an example, the noise reduction achieved with the single-layer error microphones is 14.4 dB while that with the double-layer ones is 40.5 dB.

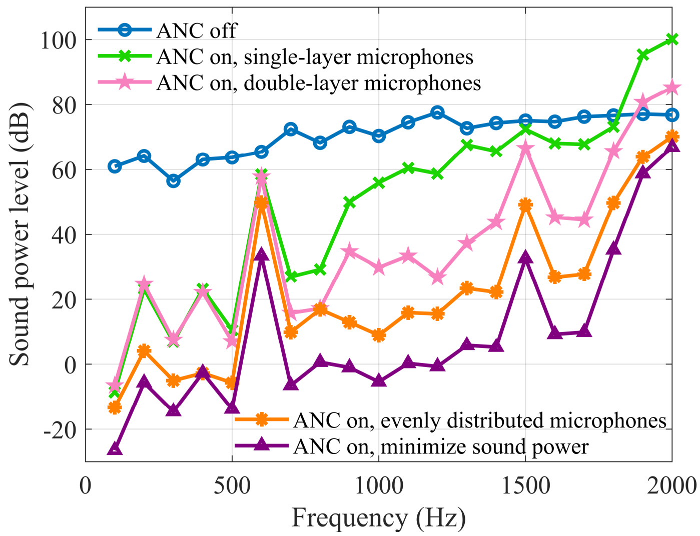


FIG. 3. (Color online) Sound power levels with and without ANC under different configurations of error microphones compared with the theoretically maximum noise reduction (minimize sound power).

The spatial distributions of the sound power level and the decibel level of the normal particle velocity at the opening with and without ANC are shown in Fig. 4. It can be seen that the effective noise reduction zones are limited with the single-layer error microphones, which are located around the edge of the opening; however, the noise reduction zones are significantly enlarged with the double-layer ones. Both the sound pressure and normal particle velocity can be significantly reduced after control with the double-layer error microphones, which is similar to the result when using acoustic energy density as the cost function to reduce noise in enclosures.[25]

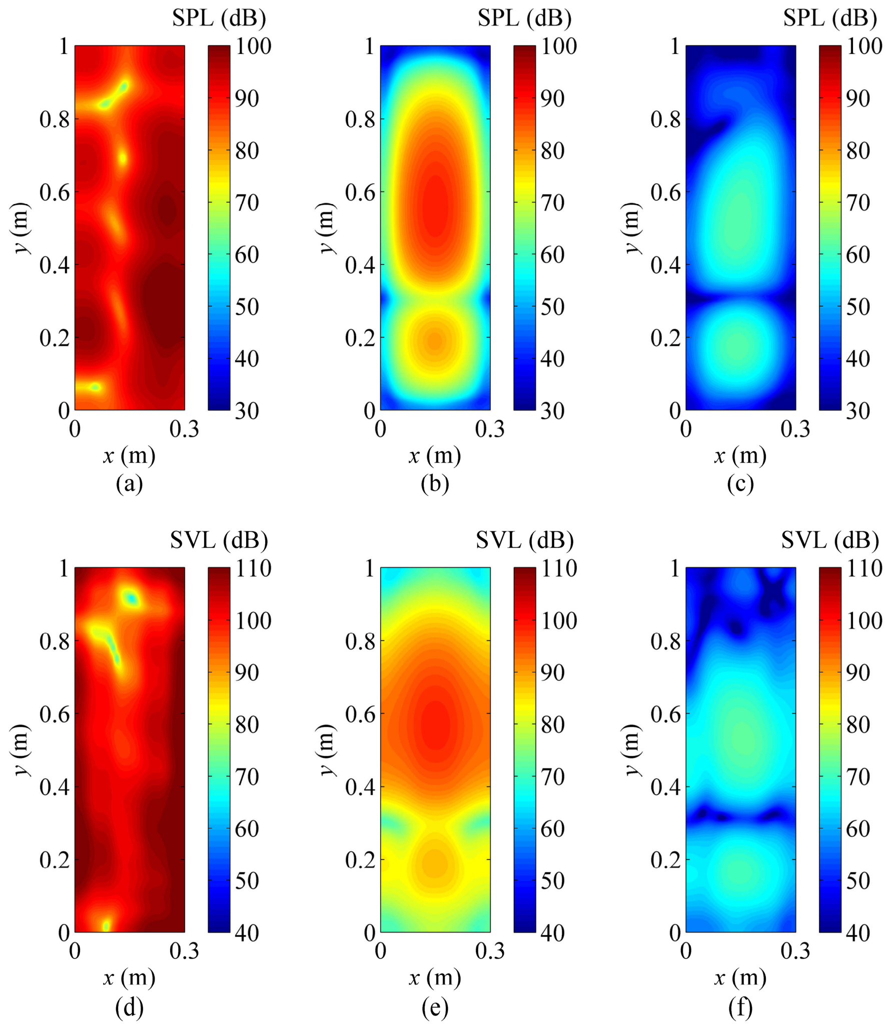


FIG. 4. (Color online) The sound power levels (SPL) at the opening with (a) ANC off; (b) ANC on, single-layer error microphones; and (c) ANC on, double-layer error microphones. The decibel levels of particle velocity (SVL) at the opening with (d) ANC off; (e) ANC on, single-layer error microphones; and (f) ANC on, double-layer error microphones. The frequency of interest is 1000 Hz.

In Fig. 3, the noise reductions at 600 Hz and 1500 Hz are limited under all the configurations because secondary sources in the same plane cannot excite some of the modes effectively.[26] The numerical simulations also show that, unlike using error microphones at the edge, the noise reduction achieved with the system using evenly distributed error microphones can approximate the maximum noise reduction (minimize sound power) if their number is sufficient.

It should be noted that double-layer error microphones do not necessarily perform better than single-layer ones. For example, if the secondary source is a monopole point source at (0.011, 0.01, 0.01) m, which is very close to the primary source, the secondary sound field matches the primary sound field very well, and the noise reduction performances of the single-layer and double-layer error microphones are similar, as shown in Fig. 5. Because strong source coupling exists in this case, the positions of error microphones are not important. In fact, using only one error microphone can achieve similar noise reduction, which is demonstrated by Fig. 5, where the noise reduction performance achieved with one error microphone at (0.1, 0.1, 0.588) m is given for comparison. In other cases where the primary and secondary sound fields do not match very well, such as when the secondary source is not located near the primary source, the double-layer error microphones at the edge outperform single-layer ones. In practical applications, there cannot be too many secondary sources, and the number depends on the frequency of the noise to be reduced, but the conclusion that double-layer error microphones outperform single-layer ones is still valid provided the primary and secondary sound fields do not match very well.

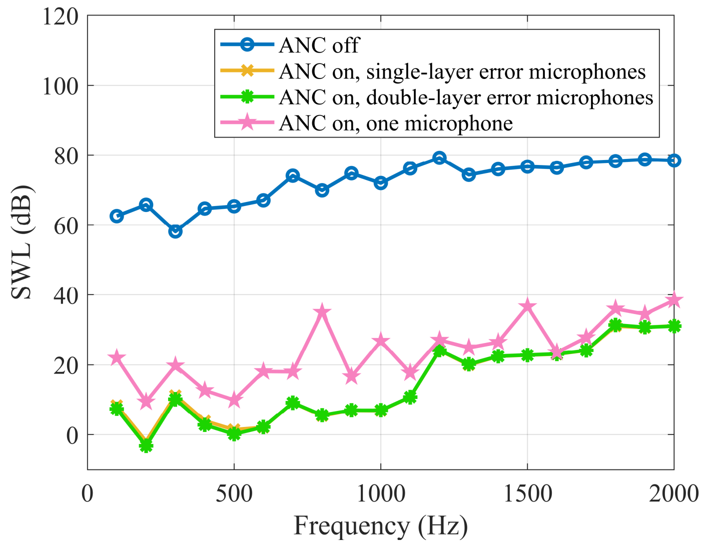


FIG. 5. (Color online) Sound power levels with and without ANC when a single secondary source is located close to the primary source.

**B. Upper-limit frequency of effective control**

There is a limitation on the control performance of the system with error microphones at the edge. The noise reduction performance achieved with error microphones at the edge will be improved at first if more secondary sources are used, but will remain stable after the number of secondary sources reaches a certain value, and this stable performance is related to the opening size. Using 20 dB as the threshold, the highest frequency at which the noise reduction is more than 20 dB with sufficient secondary sources is defined as the upper-limit frequency of effective control.

Figure 6 shows the upper-limit frequency as a function of $l_x$ when $l_y$ and $l_z$ are fixed as 1 m and 0.598 m, respectively. The primary source is located at (0.01, 0.01, 0.01) m and the secondary sources are evenly distributed in the $z$ = 0.448 m plane. The error microphones in the single-layer system are at the edge of the $z$ = 0.588 m plane and those in the double-layer system are at the edge of the $z$ = 0.568 m and $z$ = 0.588 m planes. In Fig. 6, the upper-limit frequencies of all the systems decrease with $l_x$, and the system with double-layer error microphones has higher upper-limit frequencies than that with single-layer error microphones.

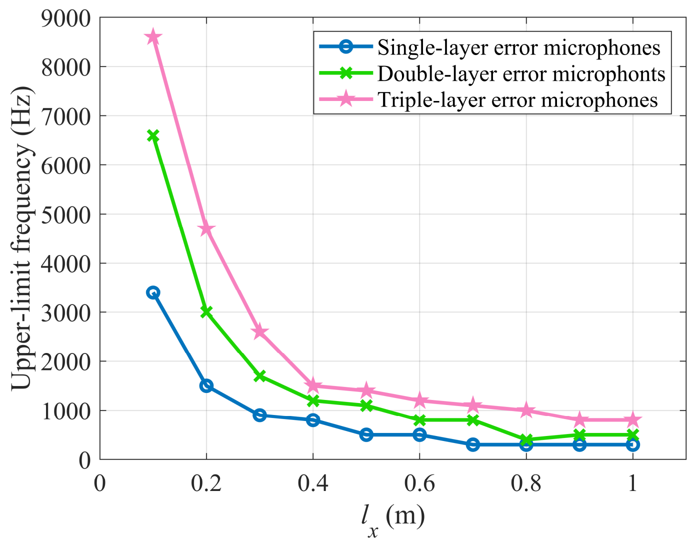


FIG. 6. (Color online) Upper-limit frequencies of effective control as a function of $l_x$ when the secondary sources are evenly distributed in $z$ = 0.448 m plane.

It can also be observed from Fig. 6 that the upper-limit frequency is mainly determined by the smaller side of the opening for a flat opening. For the system with single-layer error microphones, the wavelength of the upper-limit frequency is approximately the length of the smaller side of the cavity opening, while that for the system with double-layer error microphones is approximately half of this length. Introducing a third layer of error microphones at the edge can further increase the noise reduction achieved by error microphones at the edge. If more error microphone layers are applied, the upper-limit frequency can be improved as well, as shown by the curve corresponding to triple-layer error microphones in Fig. 6.

The cavities investigated here are only examples for illustrating the concept and to show that double-layer error microphones at the edge perform better than single-layer ones. Because the upper-limit frequency is related to the size of the opening, such a double-layer error microphone arrangement can be adjusted for applications on openings with different dimensions, and the methodology reported in this paper can be used in other specific designs.

If the secondary sound field closely matches the primary sound field, then there is little difference between the performances of using single-layer and double-layer error microphones at the edge. For example, when the secondary source is at (0.015, 0.01, 0.01) m, which is only 0.005 m away from the primary source, the upper-limit frequency achieved with a single-layer or double-layer system remains at 3400 Hz and this frequency does not change with the size of the opening. In this case, strong coupling between the primary and secondary source exists and the upper-limit frequency of effective control is determined by the distance between the primary and secondary sources, so the configuration of error microphones does not have a significant effect on the noise reduction performance. If the secondary sources cannot be placed in the proximity of the primary source, then the secondary sound field cannot match the primary sound field, and the configuration of error microphones affects the upper-limit frequency.

The upper-limit frequencies for more complicated primary sound fields are shown in Fig. 7. The multiple primary sources in the simulations are 27 monopole point sources distributed in a 0.1 m × 0.1 m × 0.1 m cuboid located from (0.01, 0.01, 0.01) m to (0.11, 0.11, 0.11) m with random amplitudes and phases. The results for one primary source at (0.01, 0.01, 0.01) m are also included in Fig. 7 for comparison.

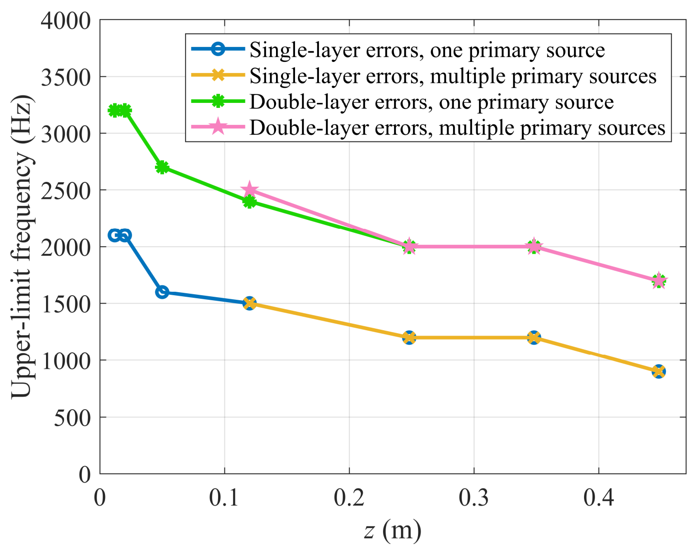


FIG. 7. (Color online) Upper-limit frequencies as a function of the plane the secondary sources are located in.

It can be seen from Fig. 7 that the upper-limit frequencies for one primary source and multiple primary sources are almost the same, which indicates that the primary sound field does not affect the upper-limit frequency, but the positions of secondary sources do have an impact on the upper-limit frequencies. As shown in Fig. 7, the upper-limit frequencies decrease with $z$, which is the plane the secondary sources are located in. It indicates that the noise reduction decreases as the secondary sources move farther away from the primary source, and the reason is weaker coupling. In any case, the upper-limit frequency of the system with double-layer error microphones at the edge is always higher than that of the system with single-layer ones.

## IV. EXPERIMENTS

The experiments were carried out in the anechoic chamber of Nanjing University to support the numerical simulation results. A panoramic view of the experimental setup is shown in Fig. 8(a). The cavity size is 0.432 m × 0.67 m × 0.598 m, and the opening is embedded on a baffle 2.4 m × 2.4 m in size. Ten microphones fixed on a semi-spherical frame with a radius of 1.5 m were used to measure the sound power levels with and without control according to ISO 3744.[11]

In the experiments, 32 secondary sources were evenly distributed in the plane 0.15 m below the opening and there were 32 error microphones in the system. Three configurations of error microphones: evenly distributed, single-layer and double-layer were investigated and their layouts on the cavity opening are shown in Figs. 8(b)–(d). The single-layer and evenly distributed error microphones were installed in the opening plane. In the double-layer system, two layers of error microphones were installed, one at the opening and the other one in the plane 0.02 m below it. A loudspeaker inside the open cavity was used as the primary source to generate a tonal sound field. The waveform synthesis algorithm was used in the experiments; it applied the internally synthesized tonal signal as the reference signal, so no reference microphone is required here.[27]

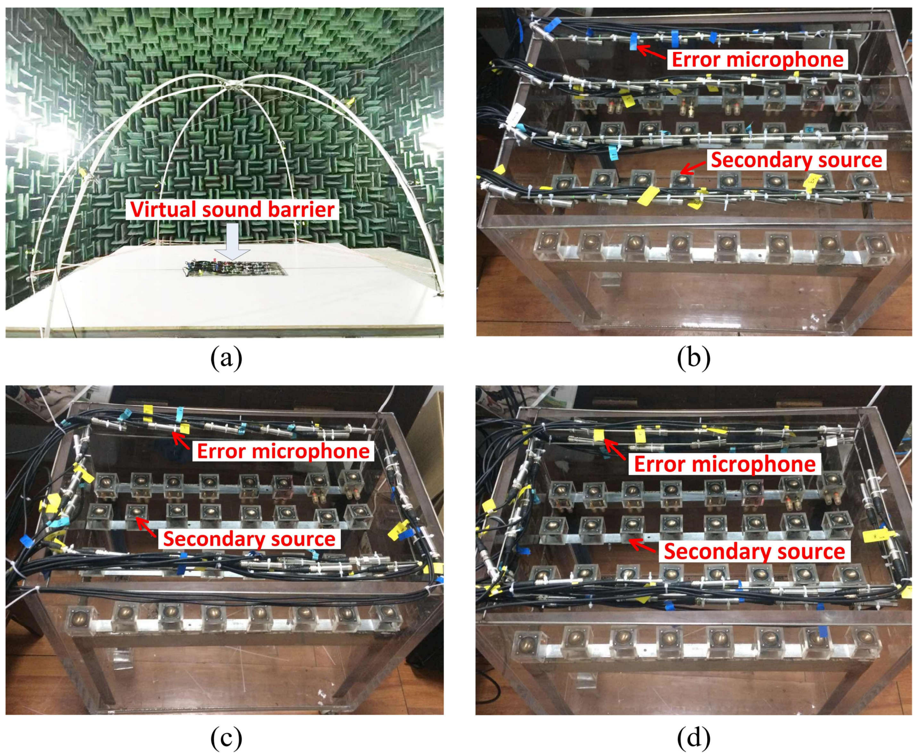


FIG. 8. (Color online) Photos of the experimental setup: (a) a panoramic view of the anechoic chamber, (b) evenly distributed error microphones, (c) single-layer error microphones at the edge, and (d) double-layer error microphones at the edge.

The sound power levels with and without control measured in the experiments are shown in Fig. 9(a). It is clear that the system with evenly distributed error microphones has the highest noise reduction among the three configurations. The system with double-layer error microphones perform better than that with single-layer ones at most frequencies between 460 Hz and 1000 Hz. This is similar to the numerical simulation results shown in Fig. 9(b).

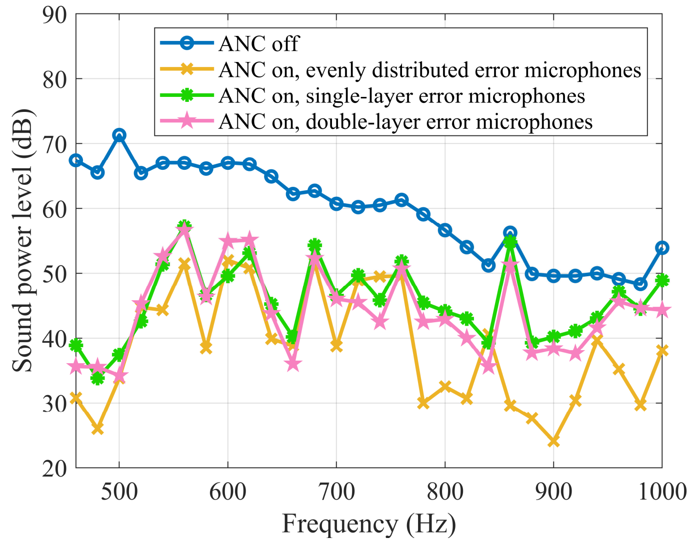


(a)

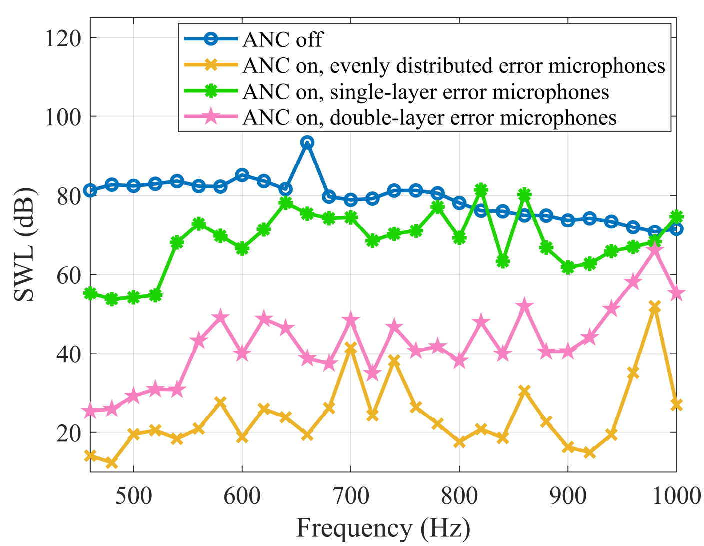


(b)

FIG. 9. (Color online) (a) Sound power levels with and without ANC measured in the experiments. (b) Simulation results on the experimental setup.

Unfortunately, the advantage of using double-layer error microphones over using single-layer ones is not as apparent as that in the numerical simulations. There are two possible reasons. One is that the sensitivities of the error microphones are different in the experiments. Because the sum of the squared electric signals picked up by the error microphones was minimized by the active controller, instead of the sum of the squared sound pressures, the noise reduction performance is deteriorated. The other possible reason is that the error microphones in the experiments were not rigorously fixed at their intended positions because of the limited space to install them.

Figure 10 shows the numerical simulation results when errors of the microphone sensitivities and positions are considered. The sensitivities of the error microphones used in the experiments ranged from 22.5 mV/Pa to 39.0 mV/Pa. The maximum error of microphone locations was 1 cm in each direction from where they were supposed to be. It can be seen from Fig. 10 that with these two factors considered, the difference between the noise reduction achieved with double-layer and single-layer error microphones become less apparent, which demonstrates that these two explanations are reasonable.

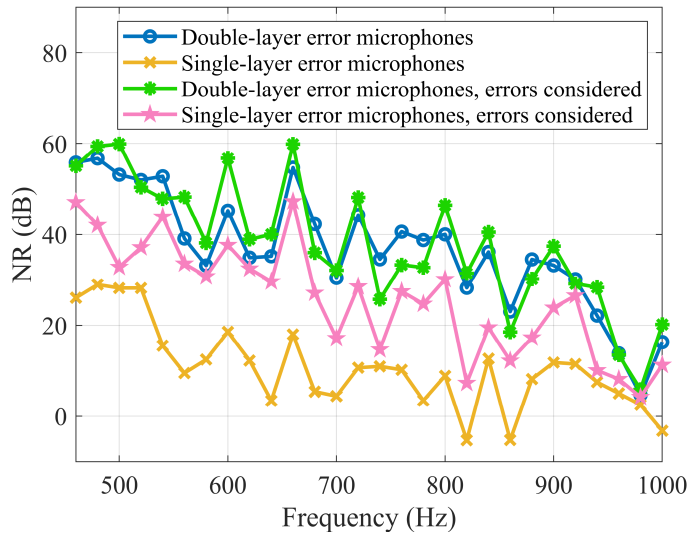


FIG. 10. (Color online) The noise reductions obtained from original numerical simulations and the numerical simulation results with errors of microphone sensitivities and locations considered.

## V. CONCLUSIONS

A boundary error sensing strategy with error microphones at the edge of the cavity opening is proposed to replace the traditional evenly distributed arrangement. It is found that the system with double-layer error microphones at the edge perform better than that with single-layer ones. The reason is that double-layer error microphones enlarge the effective noise reduction zone at the opening. Unlike the system with evenly distributed error microphones, there exists an upper-limit frequency of effective control for the system with error microphones at the edge. Generally, if the secondary sound field cannot match the primary sound field, the upper-limit frequency of effective control is related to the opening size and more error microphone layers can increase the upper-limit frequency. Experimental results in an anechoic chamber demonstrated the validity of the numerical simulation results. Future work includes combining double-layer secondary sources at the edge with double-layer error microphones at the edge to constitute an almost invisible noise reduction system that has little effect on lighting, natural ventilation, and access through the opening.

## ACKNOWLEDGEMENTS

This research was supported by the National Science Foundation of China (11474163, 11874218) and under the Australian Research Council's Linkage Projects funding scheme (LP140100987). The authors would also like to thank Mr. Kang Wang for his help with the experiments.

# REFERENCES


[1] J. Moore and R. Lyon, "Resonant porous material absorbers," J. Acoust. Soc. Am. **72**(6), 1989−1999 (1982).

[2] J. Kang and M. Brocklesby, "Feasibility of applying micro-perforated absorbers in acoustic window systems," Appl. Acoust. **66**, 669−689 (2005).

[3] C. Field and F. Fricke, "Theory and applications of quarter-wave resonators: a prelude to their use for attenuating noise entering buildings through openings," Appl. Acoust. **53**, 117−132 (1998).

[4] P. Nelson and S. Elliott, *Active Control of Sound*, Academic Press, (1992).

[5] S. Ise, "The boundary surface control principle and its applications," IEICE Trans. Fundamentals **E88-A**, 1656−1664 (2005).

[6] M. Nishimura, K. Ohnishi, N. Kanamori and K. Ito, "Basic study on active acoustic shielding," *Proceedings of Inter-noise*, Shanghai, China (2008).

[7] S. Elliott, J. Cheer, B. Lam, C. Shi and W. Gan, "A wavenumber approach to analysing the active control of plane waves with arrays of secondary sources," J. Sound Vib. **419**, 405−419 (2018).

[8] S. Wang, J. Tao, and X. Qiu, "Performance of a planar virtual sound barrier at the baffled opening of a rectangular cavity," J. Acoust. Soc. Am. **138**(5), 2836−2847 (2015).

[9] S. Wang, J. Tao, and X. Qiu, “Controlling sound radiation through an opening with secondary loudspeakers along its boundaries,” Sci. Rep. **7**: 13385, 1−6 (2017).

[10] K. Wang, J. Tao and X. Qiu, “Boundary control of sound transmission into a cavity through its opening,” J. Sound Vib. **442**, 350−365 (2019).

[11] ISO 3744: 1994, “Acoustics−Determination of sound power levels of noise sources using sound pressure−Engineering method in an essentially free field over a reflecting plane,” International Organization for Standardization, Geneva, Switzerland, (1994).

[12] H. Suzuki, M. Nakamura and J. Tichy, “An accuracy evaluation of the sound power measurement by the use of the sound intensity and the sound pressure methods,” Acoust. Sci. & Tech. **28**(5), 319−327 (2007).

[13] A. Berry, X. Qiu, and C. Hansen, “Near-field sensing strategies for the active control of the sound radiated from a plate,” J. Acoust. Soc. Am. **106**(6), 3394−3406 (1999).

[14] C. Hansen, S. Snyder, X. Qiu, L. Brooks, and D. Moreau, *Active Control of Noise and Vibration* (CEC Press, Boca Raton, FL, 2012).

[15] B. Shafer, K. Gee, and S. Sommerfeldt, “Verification of a near-field error sensor placement in active control of compact noise sources,” J. Acoust. Soc. Am. **127**, EL66−EL72 (2010).

[16] X. Qiu, C. Hansen and X. Li, “A comparison of near-field acoustic error sensing strategies for the active control of harmonic free field sound radiation,” J. Sound Vib. **215**(1), 81−103 (1998).

[17] S. Rao and T. Pan, “Optimal placement of actuators in actively controlled structures using genetic algorithms,” AIAA Journal. **29**(6), 942−943 (1991).

[18] K. Baek and S. Elliott, “Natural algorithms for choosing source locations in active control systems,” J. Sound Vib. **186**(2), 245−267 (1995).

[19] J. Xue, J. Tao and X. Qiu, “Performance of an active control system near two reflecting surfaces,” *Proceedings of the 20th International Congress on Sound and Vibration*, Bangkok (2013).

[20] J. Garcia-Bonito, S. Elliott and C. Boucher, “Generation of zones of quiet using a virtual microphone arrangement,” J. Acoust. Soc. Am. **101**(6), 3498−3526 (1997).

[21] A. Berkhoff, “Control strategies for active noise barriers using near-field error sensing,” J. Acoust. Soc. Am. **118**(3), 1469−1479 (2005).

[22] C. Peterson, A. Zander, B. Cazzolato and C. Hansen, “A moving zone of quiet for narrowband noise in a one-dimensional duct using virtual sensing,” J. Acoust. Soc. Am. **121**(3), 1459−1470 (2007).

[23] C. Fuller, C. Papenfuss and T. Saux, “Active-passive control of portable generator set radiated noise,” *Proceedings of Acoustics 2012*, Fremantle, Australia (2012).

[24] S. Elliott, P. Joseph, P. Nelson and M. Johnson, “Power output minimization and power absorption in the active control of sound,” J. Acoust. Soc. Am. **90**(5), 2501−2520 (1991).

[25] J. Parkins, S. Sommerfeldt and J. Tichy, "Narrowband and broadband active control in an enclosure using the acoustic energy density," J. Acoust. Soc. Am. **108**(1), 192−203 (2000).

[26] S. Wang, J. Tao, X. Qiu and J. Pan, "Mechanisms of active control of sound radiation from an opening with boundary installed secondary sources," J. Acoust. Soc. Am. **143**(6), 3345−3351 (2018).

[27] X. Qiu and C. Hansen, "An algorithm for active control of transformer noise with on-line cancellation path modelling based on the perturbation method," J. Sound Vib. **240**(4), 647−665 (2001).

## COLLECTED FIGURE CAPTIONS

FIG. 1. (Color online) Schematic diagrams of (a) single-layer error microphones at the edge and (b) double-layer error microphones at the edge.

FIG. 2. (Color online) The positions of error microphones in the *x*-*y* plane: (a) single-layer error microphones at the edge, (b) one of the layers of the double-layer error microphones at the edge, and (c) evenly distributed error microphones.

FIG. 3. (Color online) Sound power levels with and without ANC under different configurations of error microphones compared with the theoretically maximum noise reduction (minimize sound power).

FIG. 4. (Color online) The sound power levels (SPL) at the opening with (a) ANC off; (b) ANC on, single-layer error microphones; and (c) ANC on, double-layer error microphones. The decibel levels of particle velocity (SVL) at the opening with (d) ANC off; (e) ANC on, single-layer error microphones; and (f) ANC on, double-layer error microphones. The frequency of interest is 1000 Hz.

FIG. 5. (Color online) Sound power levels with and without ANC when a single secondary source is located close to the primary source.

FIG. 6. (Color online) Upper-limit frequencies of effective control as a function of $l_x$ when the secondary sources are evenly distributed in $z = 0.448$ m plane.

FIG. 7. (Color online) Upper-limit frequencies as a function of the plane the secondary sources are located in.

FIG. 8. (Color online) Photos of the experimental setup: (a) a panoramic view of the anechoic chamber, (b) evenly distributed error microphones, (c) single-layer error microphones at the edge, and (d) double-layer error microphones at the edge.

FIG. 9. (Color online) (a) Sound power levels with and without ANC measured in the experiments. (b) Simulation results on the experimental setup.

FIG. 10. (Color online) The noise reductions obtained from original numerical simulations and the numerical simulation results with errors of microphone sensitivities and locations considered.